Title

Split-Bregman-Based Group-Sparse Reconstruction of Multidimensional Spectroscopic Imaging Data

Authors

Burns, Brian
Wilson, Neil
Thomas, M Albert

Publication Date

2014-04-01

DOI

10.1109/isbi.2014.6867955

Peer reviewed

SPLIT-BREGMAN-BASED GROUP-SPARSE RECONSTRUCTION OF MULTIDIMENSIONAL SPECTROSCOPIC IMAGING DATA

Brian Burns[⋆]*, Neil Wilson*[†]*, M. Albert Thomas*[⋆†]

[⋆] Department of Biomedical Engineering, UCLA, Los Angeles, CA 90025 USA
[†]Bio-Medical Physics IDP, UCLA, Los Angeles, CA 90025 USA

ABSTRACT

4D Magnetic Resonance Spectroscopic Imaging data provides valuable biochemical information in vivo, however, its acquisition time is too long to be used clinically. In this paper, 4D phantom MRSI data are retrospectively under-sampled 4X, 6X, and 8X then reconstructed with Compressed Sensing and Group Sparsity. A derivation for the Group Sparse problem solution within the Split-Bregman framework is provided which allows for arbitrary, over-lapping groups of transform coefficients. Results show that Group Sparse reconstruction with over-lapping groups is more accurate at each under-sampling rate than Compressed Sensing reconstruction with superior peak line-shape and amplitude reproduction. The acceleration factors used in these experiments could potentially reduce scan times from 40 minutes to 5 minutes.

Index Terms— Group Sparsity, Compressed Sensing, Split Bregman, Convex Optimization, Spectroscopic Imaging

1. INTRODUCTION

Magnetic Resonance Imaging (MRI) exploits the resonant frequency of ^{1}H protons within water *in vivo* to generate anatomical images of the human body. Magnetic Resonance Spectroscopic Imaging (MRSI) is a similar imaging technique to MRI, however in lieu of the resonant frequency of ^{1}H protons in water, the resonant frequencies of ^{1}H protons in metabolites are used to generate a metabolic image instead. Each metabolites has a unique resonance spectrum *in vivo* caused by their molecular bonding structure, which can be used to identify and quantify their concentrations within each voxel. Using this concentration information, the biochemical compositions of healthy and diseased tissues can be determined without the need for invasive biopsies and the altered metabolism of cancers can be detected [1].

The Echo-Planar Correlated Spectroscopic Imaging (EP-COSI) MRSI pulse sequence allows for the simultaneous acquisition of two spatial and two spectral dimensions, (k_y,k_x,t_2,t_1), in one scan *in vivo* [1]. This 4D sequence provides a 2D spectrum for each voxel in a slice. The overlap of resonance peaks within a single spectral dimension is a major impediment to individual metabolites and the increased spectral dispersion offered by a second spectral dimension can disentangle complex over-lapping spectral peaks. However, 4D MRSI acquisitions are slow compared to most MRI sequences and can take up to 40 minutes, which is too long to be used on a routine clinical basis.

4D data EP-COSI acquisition is a rasterized scan that acquires a 2D spatio-temporal plane, $k_x - t_2$, from the 4D volume during each repetition time. The second spatial (k_y) and spectral (t_1) dimensions are incrementally acquired between rasters until the entire 4D volume is sampled. k_y is acquired using standard phase encoding techniques from MRI and t_1 is acquired as a series of phase shifted 1D spectra [1]. 4D EP-COSI data acquisition can be accelerated *in vivo* by non-uniformly under-sampling (NUS) the incrementally acquired dimensions, k_y and t_1. However, NUS artifacts must be removed by reconstructing the missing samples in the $k_y - t_1$ plane through non-linear, iterative reconstruction [2].

Previous work has demonstrated the feasibility of under-sampling the mixed-domain $k_y - t_1$ plane of a 4D MRSI data set and reconstructing the missing samples with Compressed Sensing (CS), Total Variation (TV) denoising, and Maximum Entropy (MaxEnt) [3, 4]. NUS rates as low as 5X were demonstrated *in vivo* and showed that it is possible to accelerate the acquisition of 4D MRSI down to a clinically acceptable 10 minutes. The current work uses the Group Sparse (GS) reconstruction method to reconstruct phantom 4D EP-COSI data sets at different NUS rates using Split-Bregman iterative reconstruction [5, 6]. The Split-Bregman algorithm has been modified to allow for arbitrary transform coefficient groupings of overlapping or non-overlapping groups and can successfully reconstruct 8X NUS MRSI data sets. The Split-Bregman algorithm has been previously used for TV-based reconstruction of NUS MRSI data [3] and for multi-channel NUS MRI data by extending the algorithm to accommodate row-wise grouping of jointly sparse samples [7].

2. THEORY

2.1. Split Bregman Algorithm

The Split-Bregman algorithm is from the class of Alternating Direction Method of Multipliers (ADMM) that split a con-

This work was supported by: a National Institute of Health (NIH) grant #1R21NS080649-01A1 (BLB), an IDEA Expansion grant from the US Army Department of Defense (DOD) Breast Cancer Research Program (BCRP)#W81XWH-10-1-0743 (MAT)

strained problem into a sequence of simpler unconstrained sub-problems [6]. It differs from continuation-based methods by keeping the values of any Lagrange multipliers fixed between iterations and modifies the data instead. This has the benefits of increased numerical stability and a lower dependence on the initial Lagrange multiplier values. If we wish to use the Split Bregman algorithm to solve the problem:

$$\begin{array}{ll} \min_{u,z} & E(u,z) \\ \text{such that} & H(u,z) \end{array} \tag{1}$$

where $E(u,z)$ is a convex, non-differentiable function and $H(u,z)$ can be assumed to be of the form $Au = z$. We first convert it to an unconstrained problem:

$$\min_{u,z} E(u,z) + \lambda H(u,z) \tag{2}$$

where conventional continuation-based methods would increase $\lambda \rightarrow \infty$ to find a solution; however, we apply the Bregman distance relaxation to equation 2 and split it into sub-problems instead. The Bregman distance for the function $E(u)$ at the point u^k is:

$$D_E^p(u,u^k) = E(u) - E(u^k) - \langle p_u^k, u - u^k \rangle \tag{3}$$

where p_u^k is the sub-gradient of $E(u)$ at u^k. The Bregman distance and iteration scheme are then applied to equation 2:

$$\begin{array}{rl} (u^{k+1}, z^{z+1}) & = \min_{u,z} D_E^p(u,u^u,z,z^k) + \lambda H(u,z) \\ p_u^{k+1} & = p_u^k - \lambda \nabla_u H(u^{k+1}, z^{k+1}) \\ p_z^{k+1} & = p_z^k - \lambda \nabla_z H(u^{k+1}, z^{k+1}) \end{array} \tag{4}$$

which is iterated over k until convergence. λ is never increased and under fairly weak assumptions on $E(u,z)$ and $H(u,z)$, $\nabla_u H$ and $\nabla_z H \rightarrow 0$ as $k \rightarrow \infty$ so that $p^{k+1} \rightarrow p^k$ and the Bregman parameters converge [6]. However, because $H(u,z)$ is of the form $Au = z$, equation 4 can be simplified:

$$\begin{array}{rl} (u^{k+1}, z^{z+1}) & = \min_{u,z} E(u,z) + \lambda \|z - Au - b^k\|_2^2 \\ b^{k+1} & = b^k + Au^{k+1} - z^{k+1} \end{array} \tag{5}$$

where b^{k+1} is a Bregman parameter that ensures $Au \rightarrow z$ as the iterations converge without increasing λ and sacrificing stability. Because $E(u,z)$ is convex and non-differentiable, equation 5 is split into u and z subproblems, which are solved independently at each iteration, decoupling u from z:

$$\begin{array}{rl} u^{k+1} & = \min_u E(u,z^k) + \lambda \|z^k - Au - b^k\|_2^2 \\ z^{z+1} & = \min_z E(u^k + 1, z) + \lambda \|z - Au^{k+1} - b^k\|_2^2 \\ b^{k+1} & = b^k + Au^{k+1} - z^{k+1} \end{array} \tag{6}$$

2.2. Group Sparse Reconstruction

GS reconstruction is an extension of CS that exploits the correlations among adjacent transform coefficients caused by their structured sparsity [5]. Structured sparsity is the tendency of large transform coefficients to be adjacent to each other and form clusters. In GS reconstruction, adjacent transform coefficients are reconstructed together in groups rather than individually, as is done in CS. By reconstructing groups of coefficients, the GS signal model correlates individual transform coefficients with their neighbors allowing them to influence each other.

GS reconstruction can be formed as a constrained convex optimization problem that uses the $l_{1,2}$-norm as the objective function instead of the l_1-norm used in CS. The $l_{1,2}$-norm is:

$$\|z\|_{1,2} = \|z_{g1}\|_2 + \|z_{g2}\|_2 + ... + \|z_{gL}\|_2 \tag{7}$$

where $z_{gi} \in \mathbb{C}^P = \{u_j, u_l ... u_n\}$ and $j,k,n \in \{S = 1...N, P \leq N\}$ is a group of transform coefficients from u. The MRSI GS reconstruction problem is then defined as:

$$\begin{array}{ll} \min_{u,z} & \|z\|_{1,2} \\ \text{such that} & \|R\mathcal{F}u - f\| \leq \sigma \\ & z = Gu \end{array} \tag{8}$$

where $u = (Y, X, F_2, F_1)$ is the reconstructed spatial, spectral-domain data, $\mathcal{F}$ is the 4D Fourier operator, R is the under-sampling mask that determines which samples were acquired in the $k_y - t_1$ plane, $f = (k_y, k_x, t_2, t_1)$ is the sampled k-space, time-domain data, G is the group matrix of 1s and 0s that determines which coefficients from u belong to each group in z [8], and σ is the standard deviation of the noise in f. The GS problem reduces to the CS problem when each group contains one coefficient, thus making $G = I$ and $z = u$. Because each transform coefficient may be within more than one group and separate reconstructions must be created for each version of that coefficient, z may contain more points than u.

2.3. Split-Bregman Based Group Sparse Reconstruction

The GS reconstruction problem is generally considered difficult to solve due to its mixed norm structure and the non-smooth nature of the $l_{1,2}$ objective function. However, by applying Split-Bregman iterative relaxation, we can solve equation 8 for the optimal MRSI reconstruction to within the standard deviation of noise with ADMM convergence guarantees. The MRSI GS reconstruction problem can be solved by the Split-Bregman algorithm by first defining equation 8 as an unconstrained problem:

$$\min_{u,z} E(u,z) + \lambda H(u,z) \tag{9}$$

where

$$\begin{array}{rl} E(u,z) & = \|z\|_{1,2} + \mu \|R\mathcal{F}u - f\|_2^2 \\ H(u,z) & = \|z - Gu\|_2^2 \end{array} \tag{10}$$

By following the process defined in equations 4-6, we can derive u and z sub-problems and a Bregman parameter update that solves the unconstrained problem in 9:

$$\begin{array}{rl} u^{k+1} & = \min_u \mu \|R\mathcal{F}u - f^i\|_2^2 + \lambda \|z^k - Gu - b_z^k\|_2^2 \\ z^{z+1} & = \min_z \|z\|_{1,2} + \lambda \|z - Gu^{k+1} - b_z^k\|_2^2 \\ b_z^{k+1} & = b_z^k + Gu^{k+1} - z^{k+1} \end{array} \tag{11}$$

where μ and λ are Lagrange multipliers. The z^{k+1} sub-problem is non-differentiable, however, its equivalent problem can be solved:

$$\begin{aligned} z^{k+1} &= \min_z \sum_{i=1}^{L} \left[\|z_{gi}\|_2 + \lambda \|z_{gi} - (Gu^{k+1})_{gi} - (b_z^k)_{gi}\|_2^2 \right] \\ &= gshrink(Gu^{k+1} + b_z^k, \tfrac{1}{\lambda}, G) \end{aligned} \tag{12}$$

where $gshrink$ is group-wise shrinkage over each group [8]. Because the u^{k+1} sub-problem is differentiable, optimality conditions can be derived for u and simplified to:

$$(\mu \mathcal{F}' R' R \mathcal{F} + \lambda G' G) u^{k+1} = \mu \mathcal{F}' R' f^i + \lambda G' \left(z^k - b_z^k \right) \tag{13}$$

where $G'G$ is a diagonal matrix with each $(G'G)_{ii}$ being the number of groups that contain transform coefficient u_i^{k+1} [8]. If each transform coefficient is in the same number of groups, so $G'G$ is a multiple of I, the left-hand side of equation 13 is circulant and can be inverted by the Fourier transform:

$$u^{k+1} = \mathcal{F}' K^{-1} \mathcal{F} \left(\mu \mathcal{F}' R' f^i + \lambda G' \left(z^k - b_z^k \right) \right) \tag{14}$$

where $K = (\mu R' R + \lambda G' G)$ is diagonal. If each transform coefficient is not in the same number of groups and $G'G$ is not a multiple of I, u^{k+1} in equation 13 can be solved for by the Gauss-Seidel method or other iterative solvers for linear systems.

Iterating the sub-problems and Bregman update over k in equation 11 solves the unconstrained problem; however, to solve the constrained problem in equation 8, an outer iteration is completed over i that updates f based on changes to u^{k+1}:

$$f^{i+1} = f^i + \left(f - R \mathcal{F} u^{k+1} \right) \tag{15}$$

The number of iterations over k is application dependent, but for the MRSI GS problem, we use 15 iterations over k for each iteration over i and iterate over i until the normalized residual error between u^{k+1} and f^i is less than $10e^{-6}$.

3. METHODS

The CS and GS reconstruction methods were compared using six fully-sampled scans of a 500mL gray matter phantom, which contained *in vivo* concentrations of brain metabolites. The scans were acquired with the volume-based 4D EP-COSI sequence on a Siemens 3T Trio scanner using a 12-channel head coil with the following parameters: 2x2x2 cm^3 voxel size, 100 t_1 increments, TR/TE/averages = 5s/23ms/1, 32x32cm^2 FOV, 256 time points along the t_2 readout, and spectral bandwidths of 1250Hz and 1190Hz along F_1 and F_2, respectively. Standard phase corrections and channel combination were applied to each scan, with no baseline corrections used. They were apodized using a sine-squared filter along t_1, and a skewed sine-squared filter with skew parameter 0.5 along t_2. Following phase correction and apodization, the fully sampled scans were retrospectively under-sampled 4X, 6X, and 8X along the $k_y - t_1$ plane using masks generated by the 2D Poisson-gap method [4].

Separate reconstructions of each NUS phantom scan were performed using CS and GS with non-overlapping groups (GS_1), and GS with 50% overlapping groups (GS_2). The grouping patterns were within the spectral domain and were comprised of equal-sized groups of $(F_2, F_1) = (8, 4)$ coefficients. Because the GS problem simplifies to the CS problem with group sizes of one coefficient, $(F_1, F_2) = (1, 1)$, the CS and GS problems were solved using the same Split-Bregman code base with different groupings.

4. RESULTS AND DISCUSSION

Figure 1 shows a select 2D COSY spectrum from the central voxel of a 4D EP-COSI gray matter phantom scan that was retrospectively under-sampled 8X using the mask shown and reconstructed by CS, GS_1, and GS_2. The 1D projections of the F_1 and F_2 dimensions are shown to the right of and above each 2D spectrum, respectively. The spectrum from the fully sampled phantom scan is shown in the top left of the figure and the 8X NUS spectrum with zeros in place of missing samples is shown to its right. The contour levels of each spectrum are the same to allow noise levels and peak heights to be compared between reconstructions. As can be seen in the 8X NUS spectrum, the broad point spread function (PSF) of the under-sampling mask caused the large diagonal peaks of NAA, Cr, Cho, and mI to alias along the F_1 dimension and obscure the much smaller NAA, Glx, mI, and Asp cross-peaks. Because of the t_1 under-sampling, the spectral peaks shown in the fully sampled F_1 projection collapsed in the 8X NUS projection. The F_1 projections of each reconstruction method show reasonable agreement with the fully sampled data set, indicating the peak energy of major diagonals, such as NAA, Cr, Cho, and mI has been deconvolved from the broad PSF by each of the reconstructions.

There are noticeable differences among the reconstructions that should be highlighted. The noise floor of the CS reconstruction is higher than GS_1 and GS_2, which makes identifying cross peaks difficult. The CS reconstructed diagonal peaks have lost their Lorentzian line-shape and the cross peaks are present but "choppy" in appearance. The GS reconstruction cross peaks and diagonals are not "choppy" in appearance, and most of the cross peaks shown in the fully sampled data set are easily identified. The peak amplitudes and line shapes of the GS_2 reconstructions are the most similar to the fully sampled data set, as shown by the low amplitude NAA and Glx cross peaks whose complex multiplet structures are well resolved in the bottom left of the spectrum.

Table 1 shows the mean metabolite peak RMSEs calculated over the central 4x4 voxels of the six NUS phantom scans and reconstructions. The RMSEs were calculated over only the metabolite peak locations in order to reduce the effects of changes to the noise distribution [4]. The lowest values calculated for each metabolite peak and NUS rate are highlighted. As can be seen, the majority of highlighted RMSEs are from the GS_2 reconstructions, which indicates that over-lapping groups may be a more reliable method of

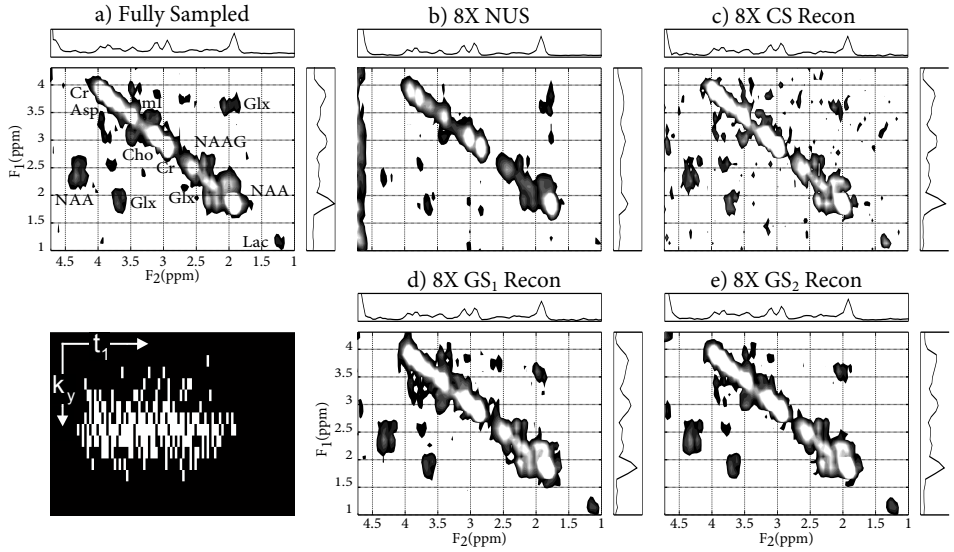

Fig. 1. Select 2D COSY spectra from the central voxel of a (a) fully sampled 4D EP-COSI brain phantom scan (b) 8X NUS and the (c) 8X CS (d) 8X GS_1 (e) 8X GS_2 reconstructions. The 8X NUS mask is shown on the left.

metabolite peak line-width and amplitude reconstruction than non-overlapping groups or CS reconstruction.

	8X NUS			**CS**		
	4X	6X	8X	4X	6X	8X
Lac 1.2	-136.5	-135.1	-134.1	-132.7	-131.6	-131.4
NAA 2.0	-108.1	-106.6	-105.5	-123.9	-120.1	-115.9
Glx 2.2	-125.2	-123.4	-122.4	-128.8	-127.5	-128.0
Cr 3.0	-110.9	-109.4	-108.3	**-127.6**	-123.0	-118.5
Cho 3.2	-114.2	-112.7	-111.6	-129.1	-126.0	-122.2
Cr 3.9	-115.3	-113.7	-112.6	-129.0	-125.7	-122.8
	GS_1			**GS_2**		
Lac 1.2	-138.5	-136.2	-135.3	**-138.8**	**-137.0**	**-135.9**
NAA 2.0	-122.5	-120.3	-116.4	**-126.6**	**-122.5**	**-117.7**
Glx 2.2	-130.9	-129.5	-127.8	**-134.5**	**-132.1**	**-129.6**
Cr 3.0	-126.2	-123.1	-118.6	-127.2	**-123.4**	**-118.8**
Cho 3.2	-124.0	-123.1	-120.4	**-128.8**	**-126.1**	**-122.4**
Cr 3.9	-129.0	-125.8	-123.0	**-131.5**	**-127.1**	**-123.7**

Table 1. Mean meatbolite peak RMSEs (dB) for the 4X, 6X, and 8X NUS and reconstructions calculated over the VOIs of the six 4D EP-COSI phantom scans.The lowest RMSE per metabolite peak and NUS rate is highlighted.

The Split-Bregman GS problem converges in fewer iterations than the CS problem, but takes more time to compute per iteration because of group-wise shrink. The current Matlab implementation of GS converges in 10-15 minutes while CS converges in 5. This is a current topic of research.

5. CONCLUSION

This preliminary work shows that GS reconstruction of 4D MRSI data set is a viable alternative to CS-based methods. The Split-Bregman-based GS algorithm was developed and evaluated on six phantom data sets at different NUS rates. The GS_2 reconstruction results demonstrated better metabolite peak reproduction and lower peak RMSEs than CS or GS_1. Further work is required to determine the optimal grouping strategies under different experimental conditions.

6. REFERENCES

[1] S Lipnick et al, "Ep-cosi: implementation and pilot evaluation in human calf in vivo," *Magn. Reson. Med.*, vol. 64, pp. 947–956, 2010.

[2] M Lustig et al, "Compressing sensing in mri," *IEEE Signal Process. Mag.*, vol. 25, pp. 72–82, 2008.

[3] JK Furuyama et al, "Application of cs to multidimensional spectroscopic imaging in human prostate," *Magn. Reson. Med.*, vol. 67, pp. 1499–1505, 2012.

[4] BL Burns et al, "Non-uniformly under-sampled multidimensional spectroscopic imaging in vivo: Maximum entropy versus compressed sensing reconstruction," *NMR in BioMed*, vol. in press, 2013.

[5] M Yuan and Y Lin, "Model selection and estimation in regression with grouped variables," *Statist. Soc. B.*, vol. 68, pp. 49–67, 2006.

[6] T Goldstein and S Osher, "The split bregman method for l1-regularized problems," *SIAM J. Imaging Sci.*, vol. 2, pp. 323–343, 2009.

[7] J Zou et al, "Split bregman algorithm for multiple measurement vector problem," *Multidim Syst Sign Process*, pp. 1–18, 2013.

[8] D Wei et al, "Group sparse optimization by alternating direction method," Tech. Rep., Dept. Comp. and App. Math., Rice U., 2011.